Supporting Information

Bio-Inspired Hydroxyl-Rich Electrolyte Additive for Highly Reversible Aqueous Zn-ion Batteries with Tough Coordination Chemistry

Jinlong Zhang[+], Qing Wu[+], Song Yang, Fusheng Luo, Yue Li, Yanhui Zhang, Kui Chen, Jun Huang, Haibo Xie,* and Yiwang Chen**

J. Zhang, Q. Wu, S. Yang, F. Luo, Y. Li, Y. Zhang, K. Chen, J. Huang, H. Xie
Department of Polymeric Materials & Engineering, College of Materials & Metallurgy, Guizhou University, Huaxi District, Guiyang 550025, P. R. China.
E-mail: huangj@gzu.edu.cn, hbxie@gzu.edu.cn.

Y. Chen
College of Chemistry and Chemical Engineering/Institute of Polymers and Energy Chemistry (IPEC)/Film Energy Chemistry for Jiangxi Provincial Key Laboratory (FEC), Nanchang University 999 Xuefu Avenue, Nanchang, 330031, China.
Key Laboratory of Fluorine and Silicon for Energy Materials and Chemistry of Ministry of Education, Jiangxi Normal University, 99 Ziyang Avenue, Nanchang, 330022, China.
E-mail: ywchen@ncu.edu.cn.

[+] These authors contributed equally to this work.

Experimental Section

Electrolyte Preparation: L-Ascorbic acid (L-Aa) were firstly mixed with deionized water by a certain mass fraction (0.5 wt%, 1.0 wt%, 2.0 wt%, 4.0 wt%), then 1 M $ZnSO_4 \cdot 7H_2O$ was into the L-Aa/H_2O hybrid solvents to form the miscible, transparent and stable electrolytes, which were labeled as $ZnSO_4$ + 0.5, 1.0, 2.0 and 4.0 L-Aa, respectively.

Cathode Preparation: The MnO_2 cathodes were synthesized via the electrodeposition method within a three-electrode system. A carbon cloth with an area of 2 cm^2, Pt foil, Ag/AgCl electrode, and a mixed solution of ammonium acetate/acetate manganese were employed as the working electrode, counter electrode, reference electrode, and electrolyte, respectively. The electrodeposition process was conducted at a consistent current density of 1 mA cm^{-2} for 15 mins using a galvanostatic charge-discharge program on an electrochemical workstation.

Materials Characterization: The XRD patterns of the samples were obtained using a Rigaku diffractometer (Mini Flex 600) equipped with Cu Kα radiation. A field emission scanning electron microscope (SEM, JEOL, JSM-7500F) was used to confirm the surface characteristics of the Zn anode. In situ optical microscopy (YUESHI YM710R) at a magnification of 10X was employed to observe the deposition behavior of Zn^{2+} on Zn foil surfaces in various electrolytes. Scanning electrochemical microscopy (SECM, CHI920D) was employed to investigate the Zn deposition behavior. X-ray photoelectron spectroscopy (XPS) was employed by Thermo Fisher Scientific K-Alpha spectrometer equipped with an Al anode for the X-ray source. Data analysis was performed utilizing Avantage software. Fourier-transform infrared spectrometry (FTIR) was employed to record the spectroscopic information of various solutions, using a Thermo Fisher Scientific Nicolet iS50 instrument, Raman microscopy was conducted using the HORIBA Scientific Lab RAM HR Evolution instrument, while liquid-state nuclear magnetic resonance (NMR) analysis was performed using the Q.one Instruments AS400 NMR spectrometer. Proton chemical shifts were obtained by preparing specimens inside a 5 mm NMR tube, where 500 μL of electrolytes were

mixed with 25 μL of deuterated oxide for locking field purposes. The proton channel resonated at a frequency of 42.58 MHz during data acquisition.

Electrochemical measurements: CR2032-type coin cells were employed to test for different electrochemical performance, which were assembled by crimping glass fibers as separators (Φ19) with 80 μL of electrolyte. The stability tests were conducted on the LANHE test system. To measure the Coulombic efficiencies (CEs), Zn//Cu asymmetrical cells were used, where a piece of Zn foil (100 μm, Φ15) served as the anode and Cu foil (10 μm, Φ15) served as the cathode. For the Zn//Zn symmetrical cells, anode and cathode are consisted by Zn foil (100 μm, Φ15). In full cells, MnO_2 works as the cathode and Zn foil (100 μm, Φ15) works as the anode. Various electrochemical tests were performed using a CHI760E.

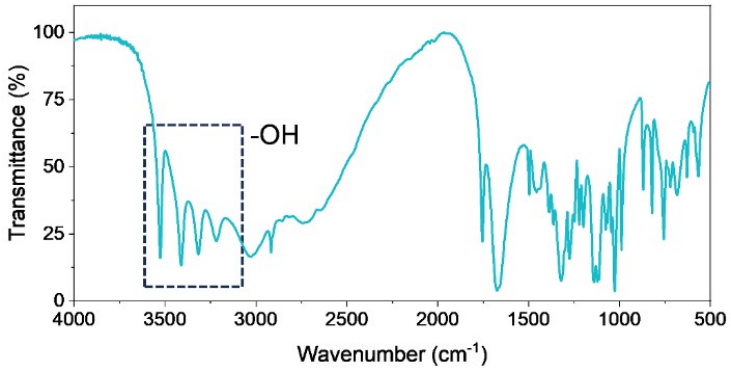

Fig. S1 The FTIR spectra of L-Aa.

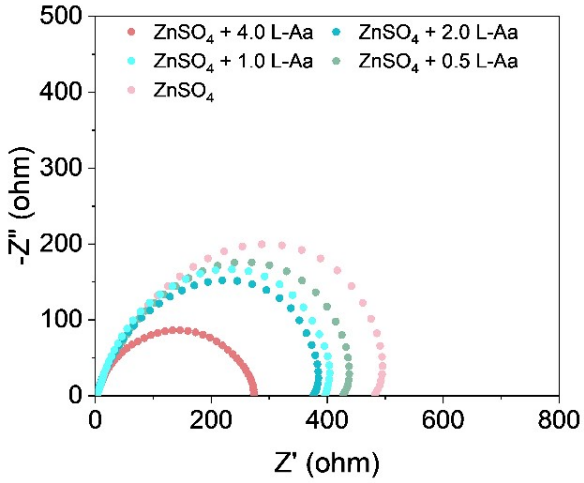

Fig. S2 Nyquist plots of Zn//Zn symmetric cells with different electrolytes.

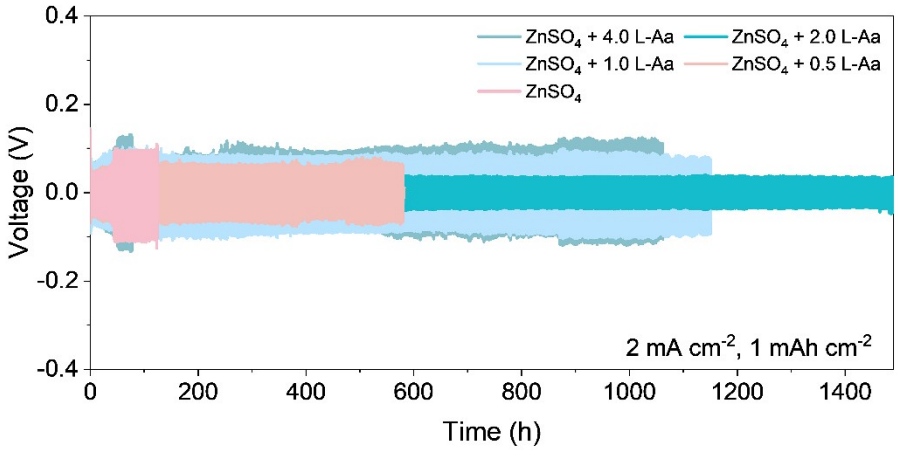

Fig. S3 The comparison of long-term cycling lifespan of Zn//Zn symmetric cells with different electrolytes.

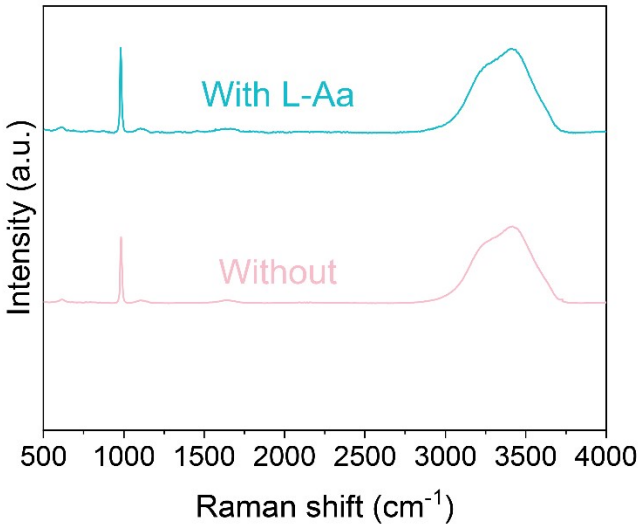

Fig. S4 The Raman spectra of electrolytes with/without L-Aa.

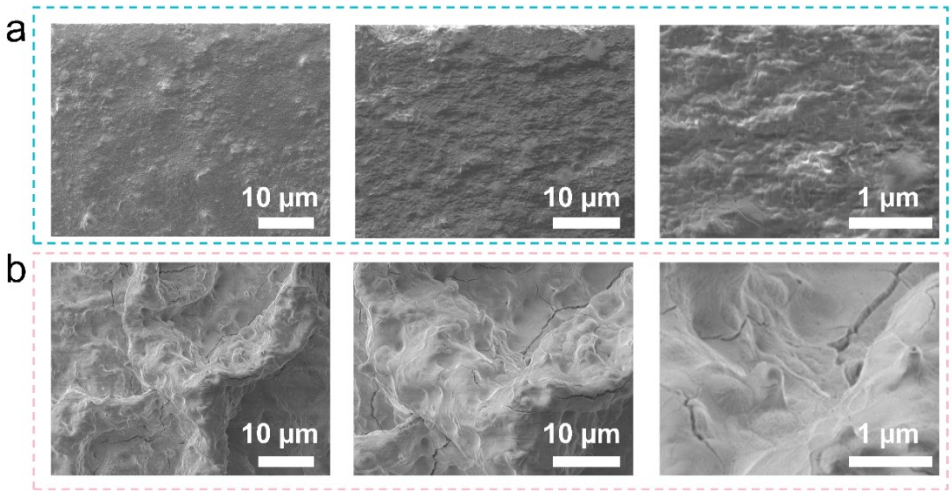

Fig. S5 The SEM images of Zn anodes soaked in electrolyte (a) with L-Aa and (b) without L-Aa for 15 days.

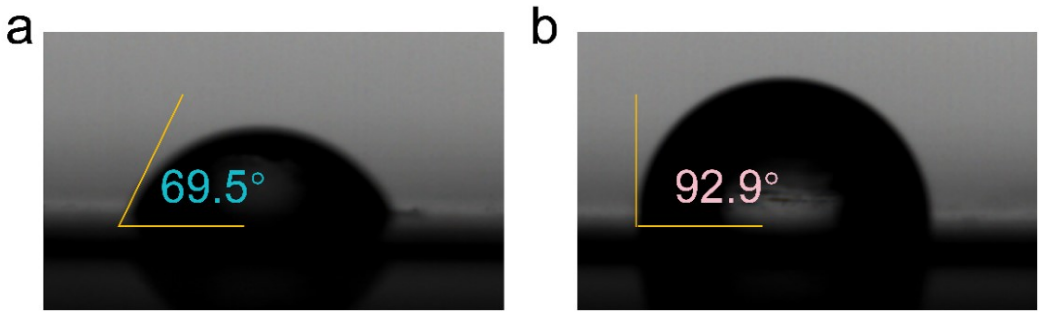

Fig. S6 Contact angle measurement of electrolyte (a) with L-Aa and (b) without L-Aa.

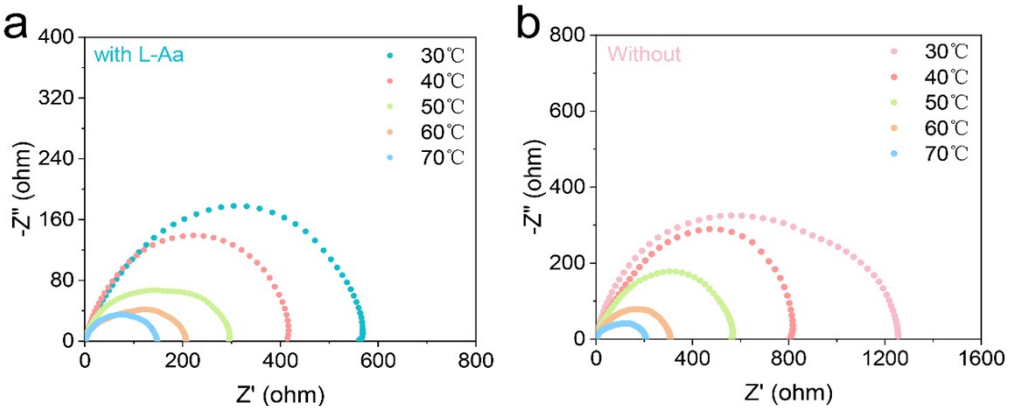

Fig. S7 Nyquist plots of Zn//Zn symmetric cells at different temperatures in the electrolyte (a) with L-Aa and (b) without L-Aa.

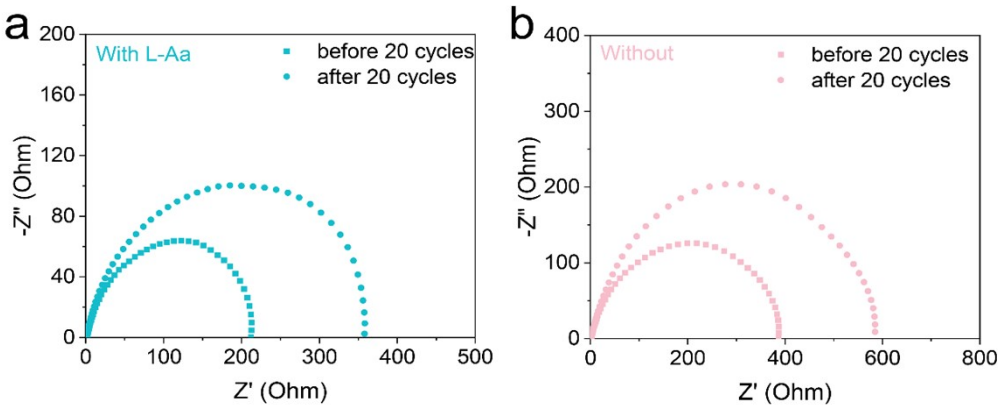

Fig. S8 Comparison for EIS of Zn//Zn symmetric cells in the electrolyte (a) with L-Aa and (b) without L-Aa before and after 20 cycles at 1 mA cm^{-2} and 1 mAh cm^{-2}.

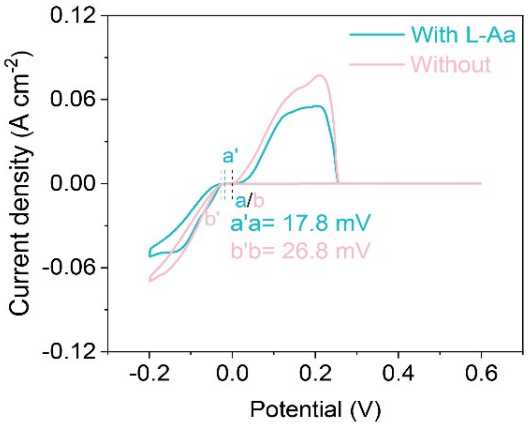

Fig. S9 CV curves of Zn//Cu asymmetric cells in the electrolyte with and without L-Aa.

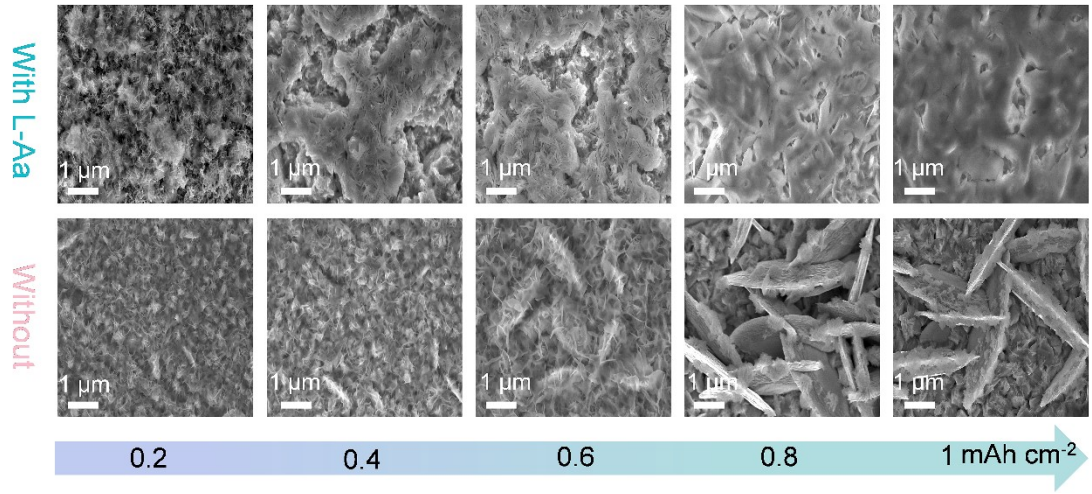

Fig. S10 The high- resolution images of *ex situ* SEM of plated Zn on Cu in the electrolyte with and without L-Aa at 0.2, 0.4, 0.6, 0.8, and 1.0 mAh cm^{-2}.

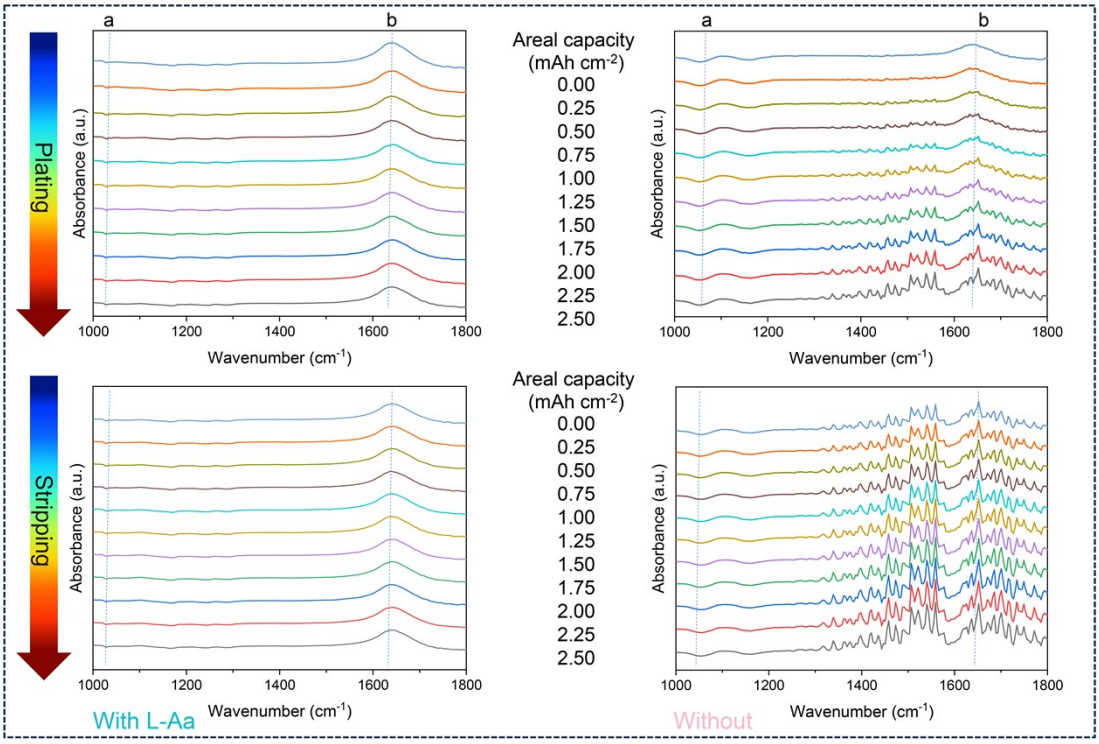

Fig. S11 *In situ* FTIR spectrum of Zn plating/stripping process with and without L-Aa at 5 mA cm^{-2} from 0 to 2.25 mAh cm^{-2}.

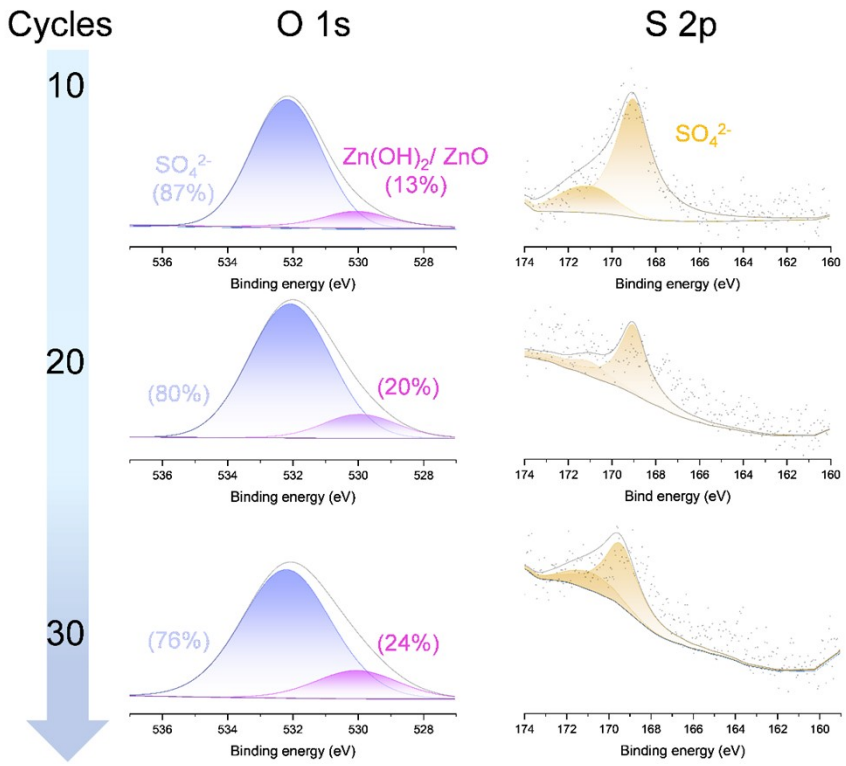

Fig. S12 *Ex-situ* XPS spectra for Zn anodes cycling 10, 20 and 30 cycles in the pure $ZnSO_4$ electrolyte at 1 mA cm^{-2} and 1 mAh cm^{-2}.

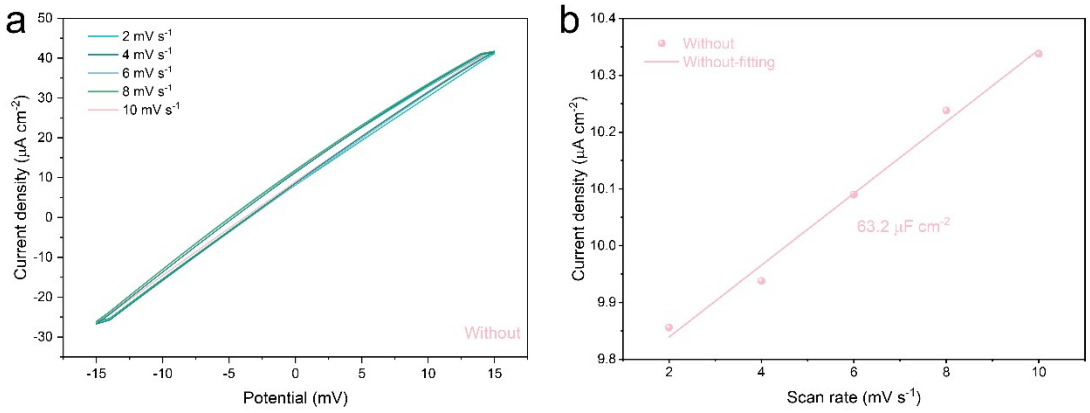

Fig.S13 EDL measurements for Zn substrates in pure $ZnSO_4$ electrolyte. (a) CV curves of Zn//Zn cells in a voltage range of -15 to 15 mV under various scanning rates. (b) Plots of capacitive currents versus scan rates.

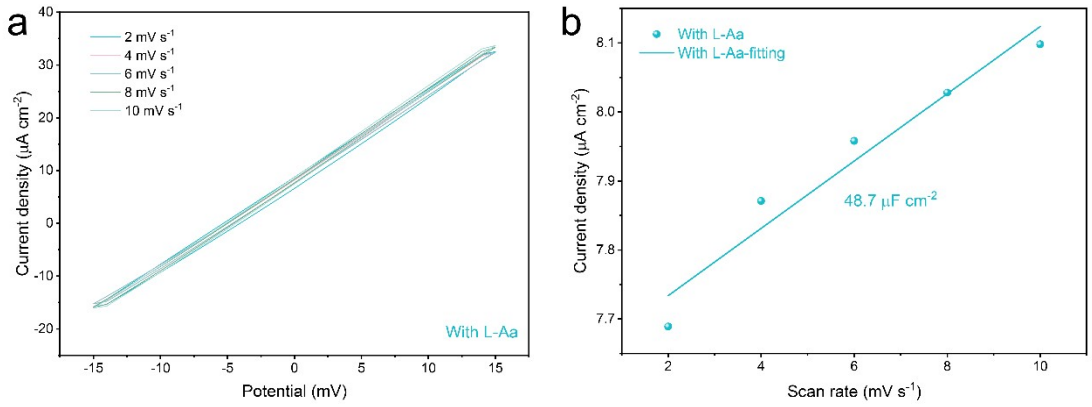

Fig.S14 EDL measurements for Zn substrates in L-Aa electrolyte. (a) CV curves of Zn//Zn cells in a voltage range of -15 to 15 mV under various scanning rates. (b) Plots of capacitive currents versus scan rates.

The capacitance (C) is determined by the linear relationship between capacitive current (i_c) and scan rate (v), which can be obtained from the slope of the i_c versus v graphs. Therefore, the EDL capacitance was calculated through the following equation:

$$C = \frac{i_c}{v}$$

Where i_c refers to the capacitive currents in CV scans. Here, we choose $i_c = (i_{0v+} - i_{0v-})/2$, meaning half value of current difference during forward scan and negative scan at 0 V. v refers to the scan rates of CV tests. Here, we selected 2, 4, 6, 8, 10 mV s^{-1} as the scan rates respectively. Corresponding CV was measured by scanning between -15 and 15 mV with Zn//Zn symmetric cells.

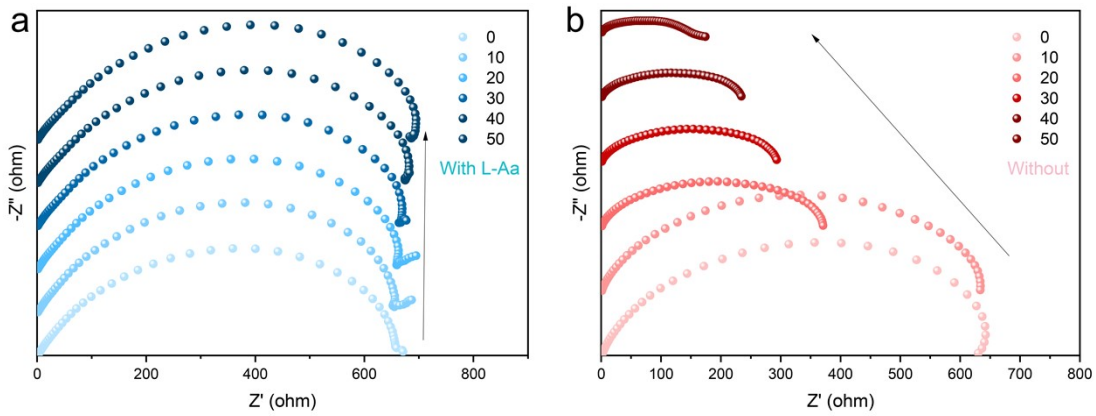

Fig. S15 *In situ* EIS of Zn//Zn symmetric cells using (a) L-Aa and (b) pure $ZnSO_4$ electrolytes during different plating/stripping cycles.

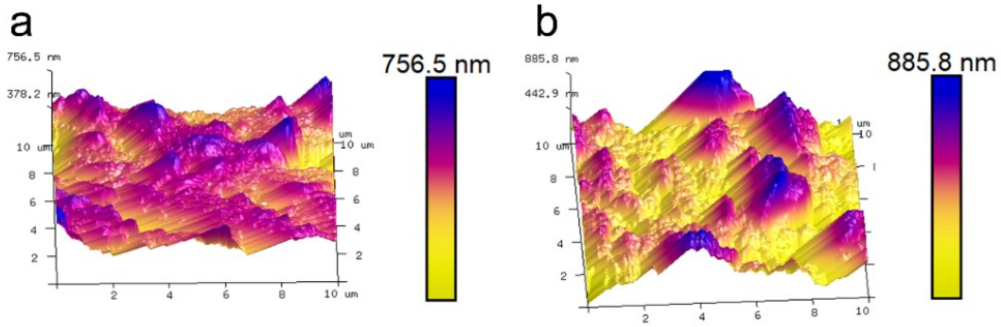

Fig. S16 AFM images of Zn anodes after 20 cycles at 1 mA cm^{-2}/1 mAh cm^{-2} in the electrolyte (a) with L-Aa and (b) without L-Aa.

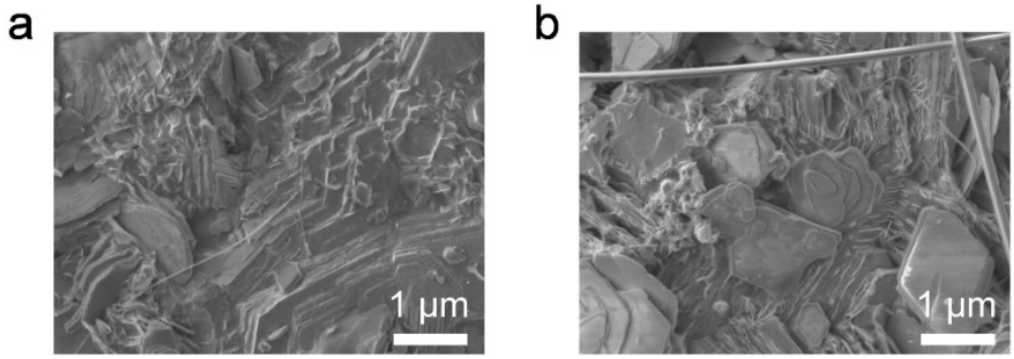

Fig. S17 SEM images of Zn anodes after 20 cycles at 1 mA cm^{-2}/1 mAh cm^{-2} in the electrolyte (a) with L-Aa and (b) without L-Aa.

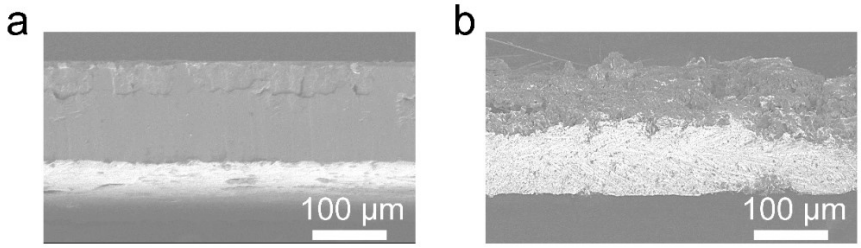

Fig. S18 Cross section SEM images of Zn anodes after 20 cycles at 1 mA cm^{-2}/1 mAh cm^{-2} in the electrolyte (a) with L-Aa and (b) without L-Aa.

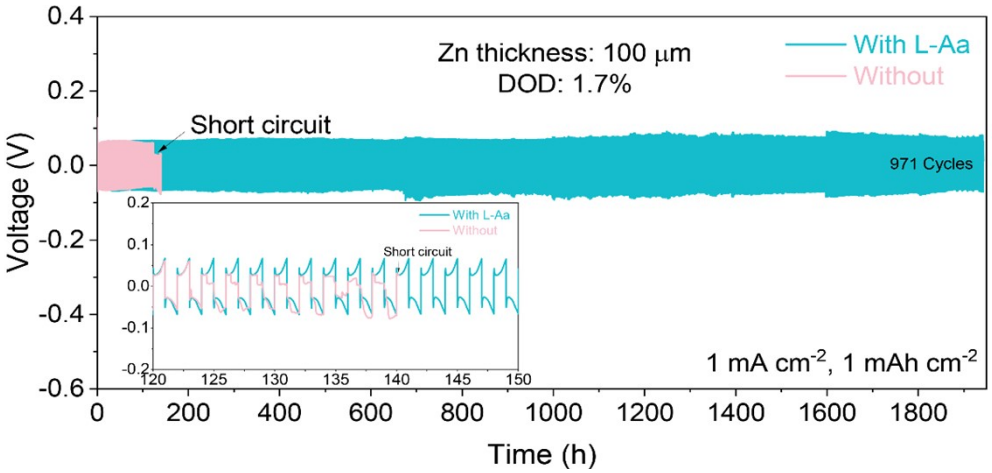

Fig. S19 Long-term cycling lifespan of Zn//Zn symmetric cells at 1 mA cm^{-2}/ 1 mAh cm^{-2} in the electrolyte with/without L-Aa.

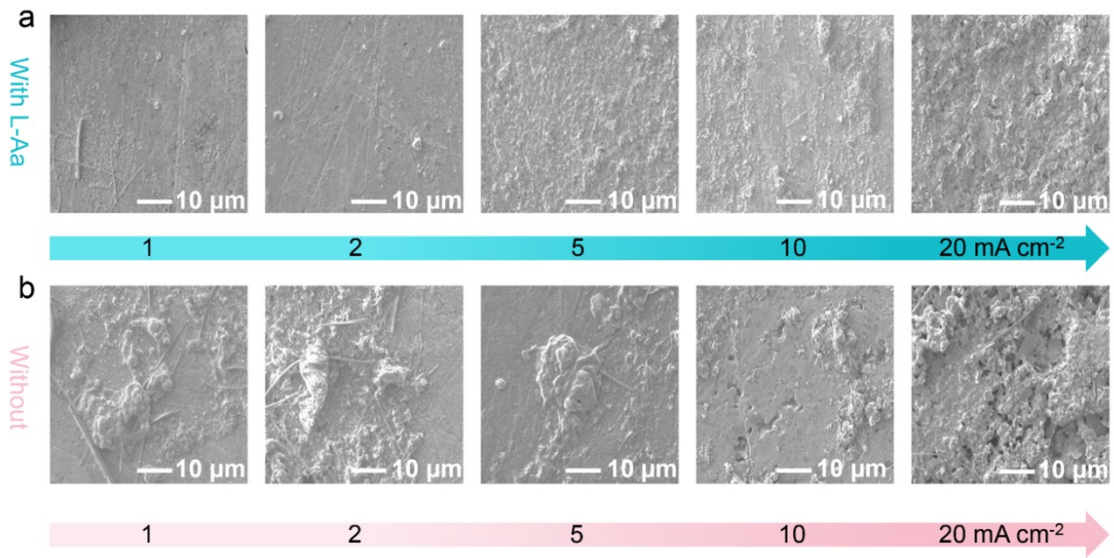

Fig. S20 *Ex situ* SEM images of Zn anodes cycled at the current density of 1, 2, 5,10, 20 mA cm^{-2} for 10 cycles in the electrolyte (a) with L-Aa and (b) without L-Aa.

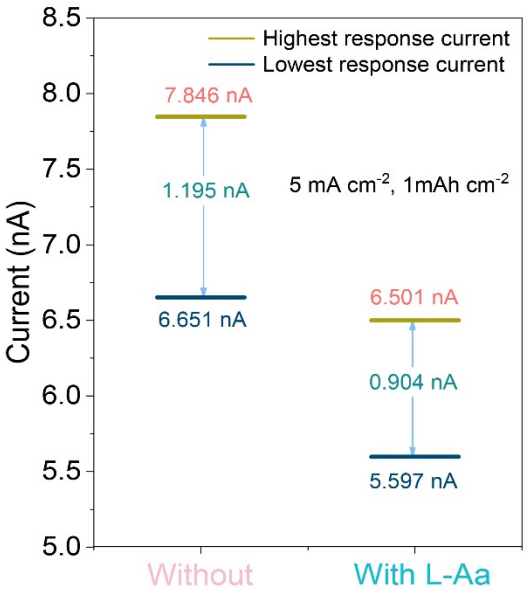

Fig. S21 The difference between the highest and lowest feedback current of Zn anode after 100 cycles at 5 mA cm^{-2} and 1 mAh cm^{-2}.

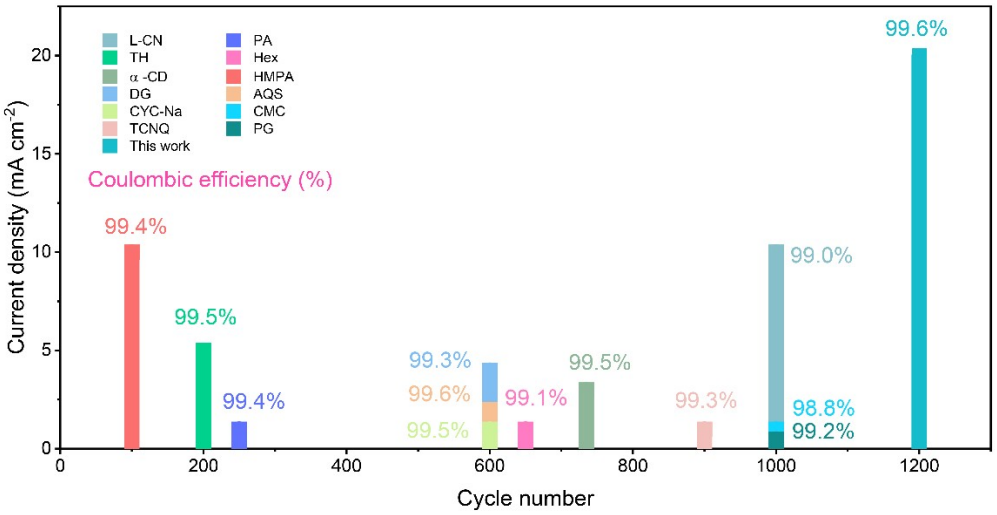

Fig. S22 Comparison of cyclic reversibility for the recent reports and this work.

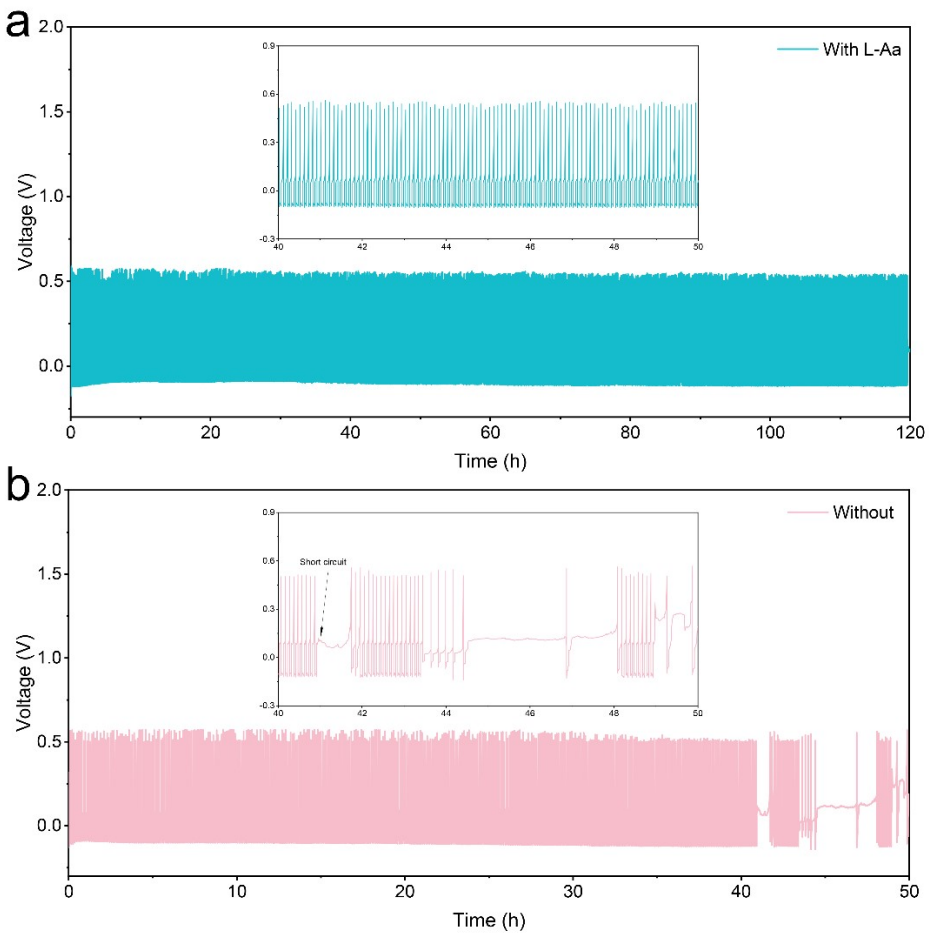

Fig. S23 Charge/discharge curves of the Zn plating/stripping process at 20 mA cm^{-2} in Zn//Cu asymmetric cells in electrolytes of (a) with L-Aa and (b) without L-Aa.

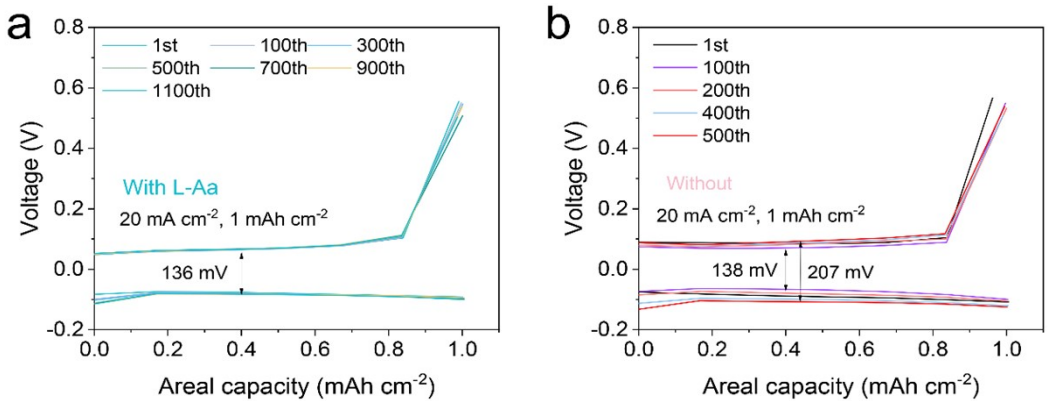

Fig. S24 The GCD profiles of Zn//Cu asymmetric cells in the electrolyte (a) with L-Aa and (b) without L-Aa at 20 mA cm^{-2} and 1 mAh cm^{-2}.

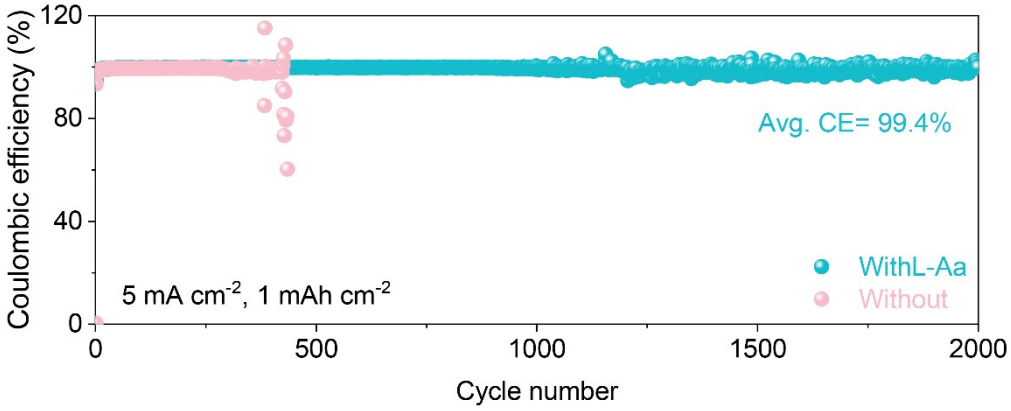

Fig. S25 CEs of Zn//Cu asymmetric cells in the electrolyte with/without L-Aa at 5 mA cm^{-2} and 1 mAh cm^{-2}.

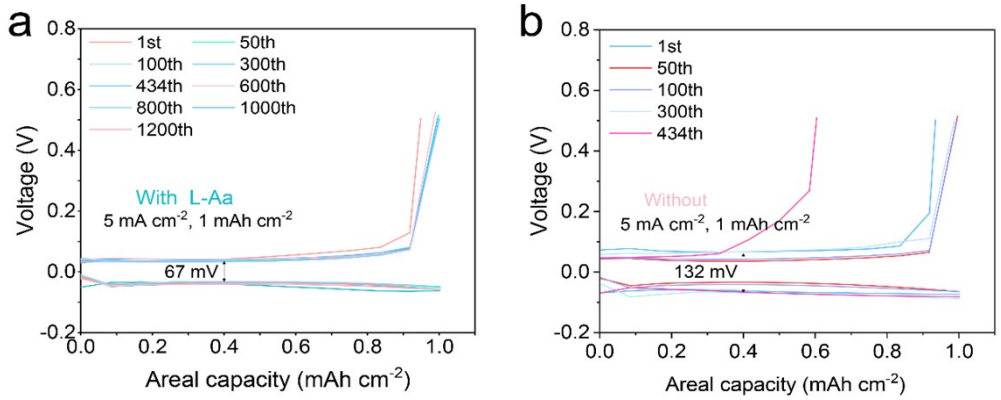

Fig. S26 The GCD profiles of Zn//Cu asymmetric cells in the electrolyte (a) with L-Aa and (b) without L-Aa at 5 mA cm^{-2} and 1 mAh cm^{-2}.

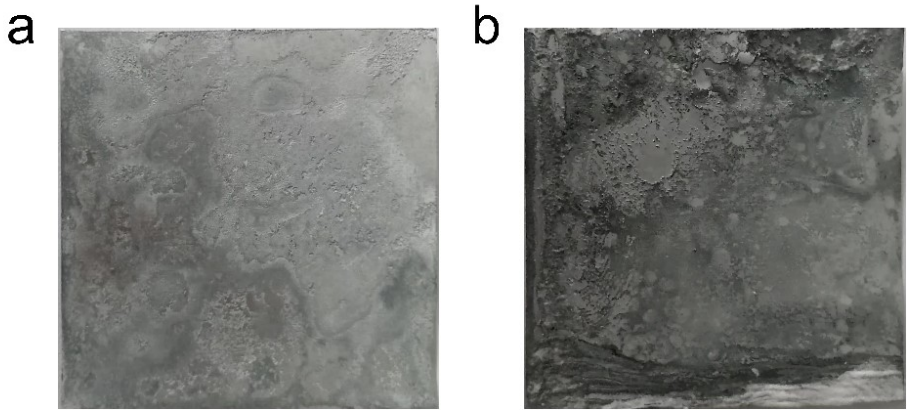

Fig. S27 Photos of the Zn anode in the Zn//Zn pouch cells in the electrolyte (a) with L-Aa and (b) without L-Aa after the cycling at 10 mA cm^{-2}, 10 mAh cm^{-2}.

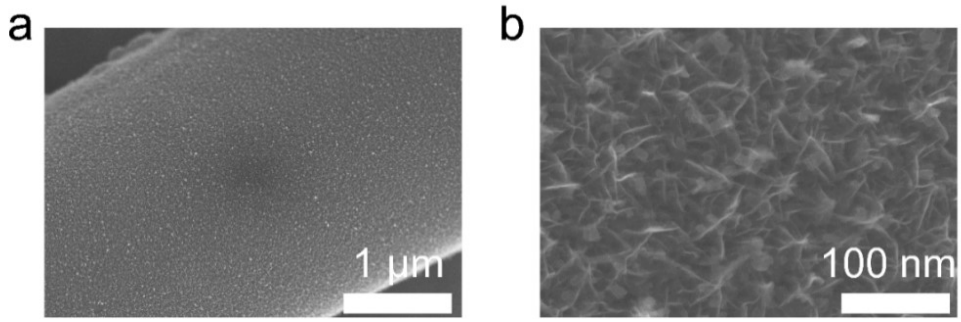

Fig. S28 (a, b) SEM images of MnO_2 cathode materials.

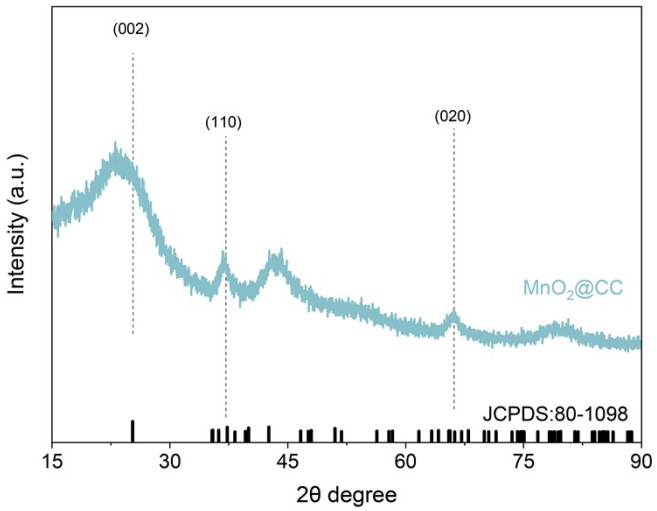

Fig. S29 The XRD pattern of MnO_2 cathode obtained by electrochemical deposition method on carbon cloth.

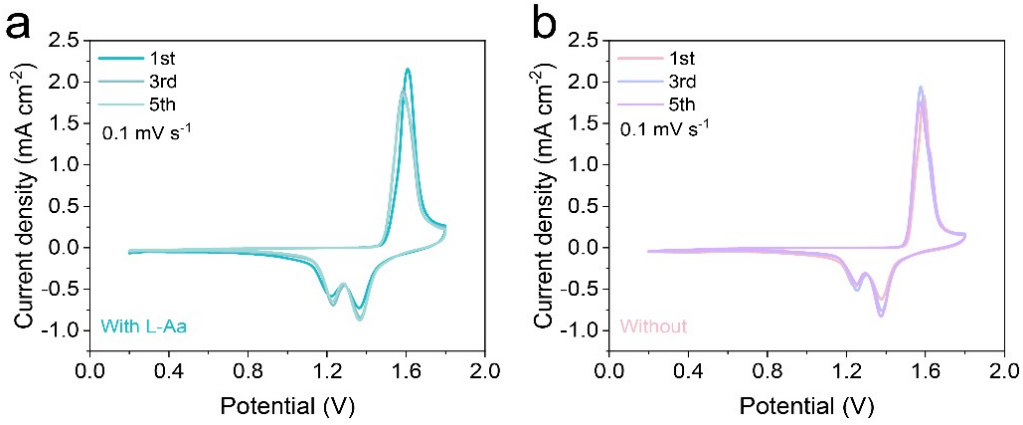

Fig. S30 CV curves of Zn//MnO_2 full cells in the electrolyte (a) with L-Aa and (b) without L-Aa at 0.1 mV s^{-1} for different cycles.

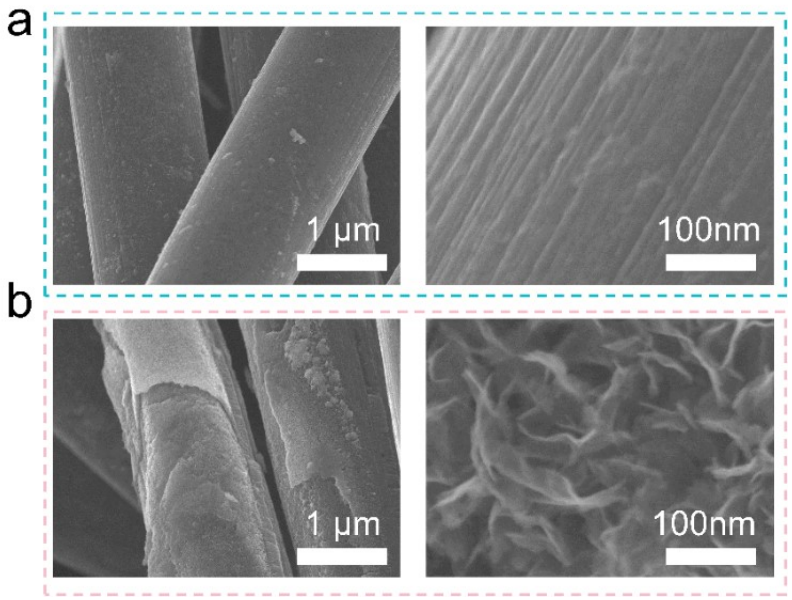

Fig. S31 SEM images of MnO_2 cathode materials after self-discharge tests in the electrolyte (a) with L-Aa and (b) without L-Aa.

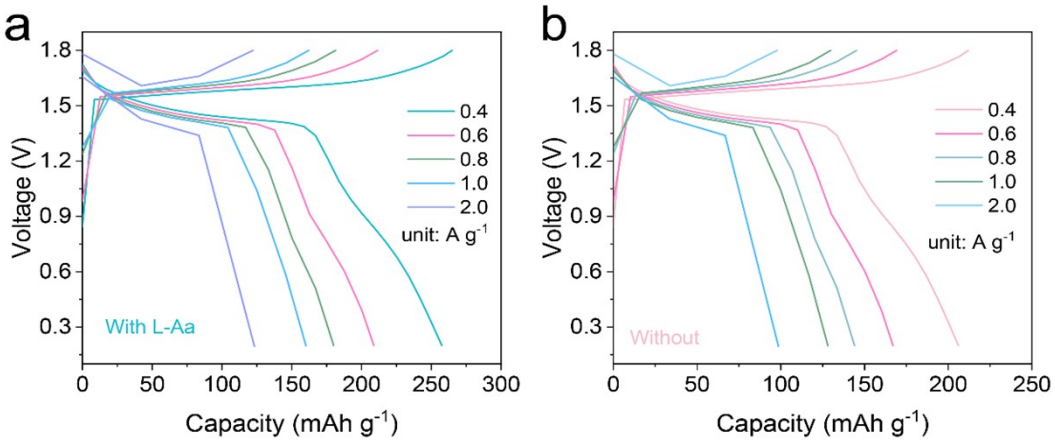

Fig. S32 GCD curves of Zn//MnO_2 full cells cycling in the electrolyte (a) with L-Aa and (b) without L-Aa under different current densities.

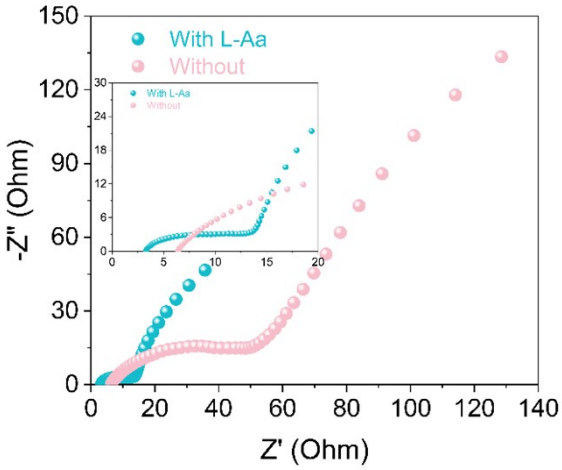

Fig. S33 EIS curves of Zn//MnO_2 full cells in the electrolyte with/without L-Aa.

Table S1.

Comparison in rate performance of Zn//Cu asymmetric cells with different additives on electrolyte additives strategy. The complete designations for the abbreviations listed under the "Additive Materials" column are L-carnitine (L-CN),[1] phytic acid (PA),[2] threonine (TH),[3] hexanehexol (Hex),[4] α-cyclodextrin (α-CD),[5] hexamethylphosphoric triamide (HMPA),[6] diethylene glycol monoethyl ether (DG),[7] sodium anthraquinone-2-sulfonate (AQS),[8] sodium cyclamate (CYC-Na),[9] propylene glycol (PG),[10] sodium carboxymethyl cellulose (CMC),[11] 7,7,8,8-tetracyanoquinodimethane (TCNQ).[12]

Additive materials	**Current density (mA cm^{-2})**	**Coulombic efficiency (%)**	**Cycle number (n)**	**Reference**
L-CN	10	98.85	1000	*Energy Environ. Sci.* 2023
PA	1	99.4	250	*Energy Storage Mater*. 2023
TH	5	99.5	200	*Nano Energy* 2022
Hex	1	99.1	650	*Energy Storage Mater.* 2023
α-CD	3	99.5	735	*Chem. Eng. J.* 2023
HMPA	10	99.4	100	*Angew. Chem. Int. Ed.* 2023
DG	4	99.7	600	*Adv. Energy Mater*. 2023
AQS	2	99.6	600	*Angew. Chem. Int. Ed*. 2023
CYC-Na	1	99.5	600	*ACS Nano* 2023
PG	0.5	99.2	1000	*Adv. Funct. Mater.* 2023
CMC	1	98.8	1000	*Energy Storage Mater*. 2023
TCNQ	1	99.3	900	*ACS Energy Lett.* 2023
L-Aa	20	99.6	1200	***This work***

Table S2.

Comparison in rate performance of Zn//Zn symmetric cells with different additives on electrolyte additives strategy. The complete designations for the abbreviations listed under the "Additive Materials" column are phytic acid,[2] threonine,[13] diethyl ether,[14] sodium cyclamate,[9] propylene glycol,[15] Dextran-Zn(CF_3SO_3)$_2$,[16] triethyl-methyl ammonium,[17] sodium anthraquinone-2-sulfonate,[18] L-carnitine,[1] hexanehexol,[4] acetylacetone,[19] hexamethylphosphoramide,[20] hexamethylenetetramine.[21]

Additive materials	**Current density (mA cm^{-2})**	**Areal capacity (mAh cm^{-2})**	**Cycle number (h)**	**Reference**
PA	1	1	1200	*Energy Storage Mater*. 2023
TH	1	1	580	*Nano Energy* 2022
Et_2O	0.2	0.2	250	*Nano Energy* 2019
CYC-Na	20	10	300	*ACS Nano* 2023
PG	1	1	1200	*Adv. Funct. Mater.* 2023
D-ZF	5	3	160	*Adv. Energy Mater*. 2023
TMA	1	0.5	360	*Adv. Energy Mater*. 2022
AQS	5	1	1100	*Angew. Chem. Int. Ed*. 2023
L-CN	8.85	8.85	1000	*Energy Environ. Sci.* 2023
Hex	5	5	425	*Energy Storage Materi.* 2023
AT	5	5	500	*Adv. Funct. Mater*. 2023
HMPA	20	4	70	*J. Am. Chem. Soc.* 2023
HMTA	5	5	600	*Adv. Energy Mater.* 2023
L-Aa	5	1	1400	***This work***
L-Aa	20	5	760	***This work***

References

1 H. Yu, D. Chen, X. Ni, P. Qing, C. Yan, W. Wei, J. Ma, X. Ji, Y. Chen and L. Chen, *Energy Environ. Sci.*, 2023, **16**, 2684-2695.

2 Y. Chen, F. Gong, W. Deng, H. Zhang and X. Wang, *Energy Storage Materials*, 2023, **58**, 20-29.

3 Z. Miao, Q. Liu, W. Wei, X. Zhao, M. Du, H. Li, F. Zhang, M. Hao, Z. Cui, Y. Sang, X. Wang, H. Liu and S. Wang, *Nano Energy*, 2022, **97**, 107145

4 Q. Hu, J. Hu, L. Li, Q. Ran, Y. Ji, X. Liu, J. Zhao and B. Xu, *Energy Storage Materials*, 2023, **54**, 374-381.

5 G. Wang, Q. Dou, P. Xiong, Q. Liu, D. Min and H. S. Park, *Chem. Eng. J.*, 2023, **457**, 141250

6 D. Wang, D. Lv, H. Peng, C. Wang, H. Liu, J. Yang and Y. Qian, *Angew. Chem. Int. Ed.*, 2023, **62**, e202310290.

7 R. Wang, Q. Ma, L. Zhang, Z. Liu, J. Wan, J. Mao, H. Li, S. Zhang, J. Hao, L. Zhang and C. Zhang, *Advanced Energy Materials*, 2023, **13**, 2302543

8 R. Sun, D. Han, C. Cui, Z. Han, X. Guo, B. Zhang, Y. Guo, Y. Liu, Z. Weng and Q. H. Yang, *Angew. Chem. Int. Ed.*, 2023, **62**, e202303557

9 G. Duan, Y. Wang, L. Sun, Z. Bao, B. Luo, S. Zheng, Z. Ye, J. Huang and Y. Lu, *ACS Nano*, 2023, **17**, 22722-22732.

10 J. Li, S. Zhou, Y. Chen, X. Meng, A. Azizi, Q. He, H. Li, L. Chen, C. Han and A. Pan, *Adv. Funct. Mater.*, 2023, **33**, 2307201

11 H. Huang, J. Yun, H. Feng, T. Tian, J. Xu, D. Li, X. Xia, Z. Yang and W. Zhang, *Energy Storage Materials*, 2023, **55**, 857-866.

12 P. Xiong, C. Lin, Y. Wei, J.-H. Kim, G. Jang, K. Dai, L. Zeng, S. Huang, S. J. Kwon, S.-Y. Lee and H. S. Park, *ACS Energy Letters*, 2023, **8**, 2718-2727.

13 Z. Miao, Q. Liu, W. Wei, X. Zhao, M. Du, H. Li, F. Zhang, M. Hao, Z. Cui, Y. Sang, X. Wang, H. Liu and S. Wang, *Nano Energy*, 2022, **97**, 107145.

14 W. Xu, K. Zhao, W. Huo, Y. Wang, G. Yao, X. Gu, H. Cheng, L. Mai, C. Hu and X. Wang, *Nano Energy*, 2019, **62**, 275-281.

15 J. Li, S. Zhou, Y. Chen, X. Meng, A. Azizi, Q. He, H. Li, L. Chen, C. Han and A. Pan, *Adv. Funct. Mater.*, 2023, **33**, 2307201.

16 J. Li, Z. Guo, J. Wu, Z. Zheng, Z. Yu, F. She, L. Lai, H. Li, Y. Chen and L. Wei, *Adv. Energy Mater.*, 2023, **13**, 2301743.

17 R. Yao, L. Qian, Y. Sui, G. Zhao, R. Guo, S. Hu, P. Liu, H. Zhu, F. Wang, C. Zhi and C. Yang, *Adv. Energy Mater.*, 2022, **12**, 2102780.

18 R. Sun, D. Han, C. Cui, Z. Han, X. Guo, B. Zhang, Y. Guo, Y. Liu, Z. Weng and Q.-H. Yang, *Angew. Chem. Int. Ed.*, 2023, **62**, e202303557.

19 H. Cao, X. Zhang, B. Xie, X. Huang, F. Xie, Y. Huo, Q. Zheng, R. Zhao, Q. Hu, L. Kang, S. Liu and D. Lin, *Adv. Funct. Mater.*, 2023, **33**, 2305683.

20 M. Kim, J. Lee, Y. Kim, Y. Park, H. Kim and J. W. Choi, *J. Am. Chem. Soc.*, 2023, **145**, 15776-15787.

21 H. Yu, D. Chen, Q. Li, C. Yan, Z. Jiang, L. Zhou, W. Wei, J. Ma, X. Ji, Y. Chen and L. Chen, *Adv. Energy Mater.*, 2023, **13**, 2300550.